HHS Public Access

Author manuscript

Nat Neurosci. Author manuscript; available in PMC 2017 July 21.

Published in final edited form as:

Nat Neurosci. 2016 October ; 19(10): 1356–1366. doi:10.1038/nn.4377.

VTA dopaminergic neurons regulate ethologically relevant sleep–wake behaviors

Ada Eban-Rothschild[1], **Gideon Rothschild**[2], **William J Giardino**[1], **Jeff R Jones**[1], and **Luis de Lecea**[1]

[1]Department of Psychiatry and Behavioral Sciences, Stanford University, Stanford, California, USA

[2]Department of Physiology and Center for Integrative Neuroscience, University of California, San Francisco, San Francisco, California, USA

Abstract

Dopaminergic ventral tegmental area (VTA) neurons are critically involved in a variety of behaviors that rely on heightened arousal, but whether they directly and causally control the generation and maintenance of wakefulness is unknown. We recorded calcium activity using fiber photometry in freely behaving mice and found arousal-state-dependent alterations in VTA dopaminergic neurons. We used chemogenetic and optogenetic manipulations together with polysomnographic recordings to demonstrate that VTA dopaminergic neurons are necessary for arousal and that their inhibition suppresses wakefulness, even in the face of ethologically relevant salient stimuli. Nevertheless, before inducing sleep, inhibition of VTA dopaminergic neurons promoted goal-directed and sleep-related nesting behavior. Optogenetic stimulation, in contrast, initiated and maintained wakefulness and suppressed sleep and sleep-related nesting behavior. We further found that different projections of VTA dopaminergic neurons differentially modulate arousal. Collectively, our findings uncover a fundamental role for VTA dopaminergic circuitry in the maintenance of the awake state and ethologically relevant sleep-related behaviors.

Motivated behaviors are critically dependent on arousal, and the capacity to organize periods of sleep and wakefulness in response to specific environmental and homeostatic conditions is essential for survival in nature. Nonetheless, little is known about the neuronal mechanisms that coordinate motivational processes with sleep–wake regulation. VTA dopaminergic neurons are central regulators of motivational processes[1–5], yet their role in

Correspondence should be addressed to L.d.L. (llecea@stanford.edu).

Note: Any Supplementary Information and Source Data files are available in the online version of the paper.

AUTHOR CONTRIBUTIONS

A.E.-R. and L.d.L. conceived and designed the study. A.E.-R. performed all experiments and analyzed data. G.R. wrote the Matlab analysis code and analyzed the fiber photometry data. W.J.G. performed histology, immunostaining and confocal imaging, and W.J.G. and A.E.-R. analyzed the immunohistochemical co-expression data. J.R.J. set up the fiber photometry rig. A.E.-R. wrote the manuscript with feedback from all the authors. L.d.L. supervised the study.

COMPETING FINANCIAL INTERESTS

The authors declare no competing financial interests.

the generation and maintenance of wake-fulness is controversial and underexplored from a causal perspective[6].

A current model for sleep–wake regulation proposes that it is governed by complex interactions between several neuronal populations that show robust arousal-state-dependent alterations in firing rate[7]. Early electrophysiological findings suggested that VTA and substantia nigra pars compacta dopaminergic neurons do not change their mean firing rate across sleep–wake states[8–11]. Moreover, lesions of VTA and substantia nigra pars compacta dopaminergic neurons result in lack of behavioral arousal but do not modify time spent in electrocortical wakefulness[12]. These findings led to the influential hypothesis that VTA dopaminergic neurons are not involved in the proper regulation of sleep–wake states and are only essential for behavioral but not electrocortical wakefulness[6,7].

In contrast, growing evidence suggests that dopamine is required for normal electrocortical sleep–wake states. Stimulants enhancing dopaminergic tone are among the most potent wake-promoting substances known[13] and their arousing effects are abolished in mice deficient in dopamine signaling[14,15]. Humans with reduced levels of dopamine reuptake transporter display altered slow-wave activity following sleep deprivation[16]. Genetically modified animal models, lesioning studies and pharmacological manipulations support a role for dopamine in arousal regulation[14,17–21], yet its source remains unclear. Extracellular dopamine levels in the nucleus accumbens (NAc) and the medial prefrontal cortex (mPFC) fluctuate across arousal states[22]. Furthermore, a more detailed examination of VTA dopaminergic neuron firing patterns revealed changes in the temporal pattern, rather than mean rate, across sleep–wake states[23]. During motivated waking and REM (rapid eye movement) sleep, VTA dopaminergic neurons are strongly activated and exhibit pronounced burst firing, whereas during quite waking and non-REM (NREM) sleep these neurons exhibit slow firing rates with an irregular pattern[23]. Taken together, these findings make VTA dopaminergic neurons appealing candidates to link motivational processes and sleep–wake regulation; however, functional proof of this hypothesis has remained lacking.

In this study, we recorded neuronal activity in VTA dopaminergic neurons of freely behaving mice using fiber photometry and combined behavioral, chemogenetic and optogenetic manipulations with polysomnographic recordings. We examined the necessity of VTA dopaminergic neurons for electrocortical and behavioral wakefulness under basal conditions and in the presence of salient stimuli related to mating, feeding and predation. We also examined the sufficiency of VTA dopaminergic neurons and their projections to generate and maintain wakefulness. We uncovered a fundamental role for VTA dopaminergic circuitry in ethologically relevant sleep-related behavior, in addition to a pivotal role in the maintenance of the behavioral and electrocortical awake state.

RESULTS

We assessed population activity of VTA dopaminergic neurons across spontaneous sleep–wake states using fiber photometry technology[24,25] by injecting a Cre-dependent adeno-associated virus (AAV) encoding the fluorescent calcium indicator GCaMP6f (AAV-DJ-EF1α-DIO-GCamP6f) into the VTA of tyrosine hydroxylase (Th)-IRES-Cre (Th-Cre)

knock-in mice ($n = 4$ mice). We implanted the mice with a fiber optic probe for subsequent delivery of excitation light and collection of fluorescent emission[24'25] and with electroencephalogram-electromyogram (EEG-EMG) electrodes for simultaneous sleep–wake recordings (Fig. 1a,b). We recorded calcium and EEG-EMG signals during the inactive, light phase in the home environment of mice. When comparing the fluorescence signal and rate of calcium transients across arousal states, we found robust alterations in *Th*$^+$ VTA population activity (Fig. 1c–f and **Supplementary Fig. 1h–k**). During NREM sleep, *Th*$^+$ VTA neurons showed a lower fluorescence and calcium transient rate than during either wake or REM sleep (Fig. 1c–e and **Supplementary Fig. 1h–k**). Notably, *Th*$^+$ VTA neurons began to decrease their activity before wake-to-NREM transitions and increase their activity before NREM-to-REM and NREM-to-wake transitions (Fig. 1f and **Supplementary Fig. 1l**). In contrast, *Th*$^+$ VTA neurons showed a higher fluorescence and calcium transient rate during REM sleep than during either wake or NREM sleep (Fig. 1c–f and **Supplementary Fig. 1h–k**), consistent with previous data[23]. These findings demonstrate that *Th*$^+$ VTA neurons change their population activity across sleep–wake states and offer a mechanistic framework for the participation of *Th*$^+$ VTA neurons in the regulation of sleep and wakefulness.

Th$^+$ VTA neurons are necessary for wakefulness

To examine the causal role of VTA dopaminergic neurons in electro-cortical and behavioral wakefulness, we employed a chemogenetic approach[26]. We injected an AAV encoding a modified inhibitory muscarinic G protein–coupled receptor (AAV5-EFlα-DIO-hM4Di-mCherry, 'hM4Di' hereafter; or the control virus AAV5-EFlα-DIO-mCherry, 'mCherry' hereafter) into the VTA of Th-Cre mice and implanted EEG-EMG electrodes (Fig. 2a,b and **Supplementary Fig. 2**). Once neurons express the hM4Di receptor they can be inhibited by systemic clozapine-*n*-oxide (CNO) administration[26].

To examine the necessity of *Th*$^+$ VTA neurons for wakefulness, we injected mice with saline or CNO (1 mg kg^{-1}; intraperitoneal injection) at the beginning of the active, dark phase (Zeitgeber time ZT 14) and monitored their EEG-EMG signals for 24 h). CNO inhibition of *Th*$^+$ VTA neurons promoted all polysomnographic characteristics of sleep (Fig. 2c,d and **Supplementary Fig. 3a,b**). In hM4Di mice, CNO administration reduced wakefulness and increased NREM and REM sleep during the 2 h following injection, as compared with saline and mCherry controls (Fig. 2d and **Supplementary Fig. 3a,b**). The EEG power spectrum during NREM and REM sleep, induced by inhibition of *Th*$^+$ VTA neurons, was similar to the spectrum displayed during spontaneous sleep (Fig. 2e – h), and NREM sleep episodes showed a typical increase in delta power with time (**Supplementary Fig. 3c**). CNO reduced the latency for NREM sleep in hM4Di mice but did not alter REM latency (Fig. 2i,j). CNO increased NREM episode duration in hM4Di mice, while leaving the number of episodes intact (Fig. 2k,l). In contrast, CNO administration increased the number of REM episodes in hM4Di mice rather than their duration (Fig. 2k,l). These findings show that *Th*$^+$ VTA neurons are necessary for the maintenance of both electrocortical and behavioral wakefulness and that their inhibition induces polysomnographic and behavioral characteristics of sleep.

Th+ VTA neurons are necessary for salience-induced wakefulness

Dopaminergic VTA neurons are activated in response to ethologically relevant salient stimuli (Fig. 3a)[1–5], yet it remains unknown whether they are necessary for the generation and maintenance of wakefulness in face of salient stimuli. We inhibited *Th*+ VTA neurons during the active (dark) phase while presenting male mice different salient stimuli. Forty-five minutes after saline or CNO administration (at ZT 13.75), we provided mCherry and hM4Di mice palatable food (6 g of high-fat chow) while simultaneously recording EEG-EMG signals for 1 h. In the presence of palatable food all three control groups were mostly awake (Fig. 3b). In contrast, CNO administration to hM4Di mice before the palatable food presentation prevented the maintenance of wakefulness and promoted NREM sleep (Fig. 3b and **Supplementary Fig. 4a,b**). When the palatable food was made inaccessible, control mice showed near-complete wakefulness and persistence in behavioral response to the stimulus (Fig. 3c, **Supplementary Fig. 4b** and **Supplementary Video 1**). CNO administration to hM4Di mice, in contrast, promoted NREM sleep and prevented the maintenance of wakefulness and persistence in behavioral response (Fig. 3c, **Supplementary Fig. 4a,b** and **Supplementary Video 2**), even after 16 h of food deprivation (Fig. 3d). Nonetheless, during a 1-h accessible palatable food test, control and CNO-treated hM4Di mice consumed similar amounts of high-fat chow (Fig. 3e), suggesting that the reduction in wakefulness and increase in sleep following *Th*+ VTA neuron inhibition was not due to the mouse's inability to perceive the salience of the stimulus.

Next we examined the necessity of *Th*+ VTA neurons to wakefulness in face of mating-related stimuli. In the presence of an adult female mouse, either freely moving or restricted to a mesh cage, all three control groups were mostly awake (Fig. 3f,g, **Supplementary Fig. 4b** and **Supplementary Videos 3** and **5**). In contrast, CNO administration to hM4Di mice prevented the maintenance of wakefulness and promoted NREM sleep (Fig. 3f,g, **Supplementary Fig. 4a,b and Supplementary Videos 4** and **6**). Nevertheless, during test periods where they remained awake, CNO-treated hM4Di mice showed typical mating related-behaviors (**Supplementary Video 4**), strengthening the premise that the reduction in wakefulness following *Th+* VTA neurons inhibition was not due to the inability to perceive the salience of the stimulus.

Lastly, we examined the necessity of *Th*+ VTA neurons to arousal in face of an aversive stimulus. As with the appetitive stimuli, CNO administration to hM4Di mice before the presentation of predator odor prevented the maintenance of wakefulness and promoted NREM sleep (Fig. 3h and **Supplementary Fig. 4a,b**).

Together these findings demonstrate that *Th*+ VTA neuron inhibition prevents a proper arousal response in face of some of the most salient stimuli for animals, related to feeding, reproduction and predation. Our findings strongly suggest that *Th*+ VTA neurons have a key role in salience-induced arousal.

Inhibition of *Th*+ VTA neurons prompts nest-building behavior

Sleep typically occurs in a species-specific site, commonly the home environment or nest[27–29]. We thus wished to examine whether sleep induced by inhibition of *Th*+ VTA

neurons was context specific and would persist in mice removed from their home environment and transferred to a novel one. We transferred mCherry and hM4Di mice to a new cage containing *ad libitum* food and water and a 3 g Nestlet (a pressed cotton square used for nest construction) 45 min after saline or CNO administration (ZT 13.75) while simultaneously recording their EEG-EMG signal for 1 h (Fig. 4a). CNO administration to hM4Di mice slightly increased NREM sleep compared to the control groups, which were continuously active during the entire test period (Fig. 4b). CNO-treated hM4Di mice slept during only 14.9% ± 5.9 of the test period in the novel environment, substantially less than in the familiar home environment (Fig. 3b–d,f–h), and only toward the end of the hour (mean latency for NREM episode: 46.57 ± 3.12 min; **Supplementary Fig. 5a**). Notably, CNO-treated hM4Di mice were mainly engaged in nest-building during the test period (**Supplementary Video 7**), and we found newly constructed nests at the end of the hour in all CNO-treated hM4Di mice cages (Fig. 4c,d). In contrast, mice from all three control groups left their newly provided nesting material practically untouched during the test period (Fig. 4c,d and **Supplementary Video 8**). Nesting behavior induced by CNO was indistinguishable from the goal-directed behavior observed during normal nest-building and included pulling, carrying, fraying, push-digging, sorting and fluffing of nesting material and bedding (**Supplementary Video 7**), as previously described[30]. To exclude the possibility that nest construction was induced by hypothermia, we monitored core body temperature for 4 h following CNO administration, finding no decrease in body temperature from baseline in either mCherry or hM4Di mice (**Supplementary Fig. 5b**).

We next wished to examine whether the nest-building behavior we observed was a response to the lack of a nest in the new environment or was a nonspecific, stereotypic behavior elicited by *Th*$^{+}$ VTA neurons inhibition, unrelated to sleep. We thus repeated the first experiment but here we transferred test mice together with their old nest to the new environment (Fig. 4e). All control groups were continuously active during the test period, scattering the material of their old nest about the cage (Fig. 4f,g and **Supplementary Video 9**). In contrast, in the presence of their old nest, CNO-treated hM4Di slept as in their home environment (Fig. 3b–d,f–h) and significantly more than in a new cage without their nest (one-tailed *t*-test; $t_6 = 2.5$, $P = 0.02$). Moreover, in the presence of their old nest, CNO-treated hM4Di left their newly provided nesting material practically untouched (Fig. 4g and **Supplementary Video 10**). Together, our findings strongly indicate that, in addition to promoting sleep, *Th*$^{+}$ VTA neuron inhibition unleashes a complex, ethologically relevant sleep-related behavior in a context-dependent manner.

We next wished to determine population activity of *Th*$^{+}$ VTA neurons during nest-building behavior. In this experiment, we sought to induce nest-building without transferring the mice to a new environment or introducing novel objects (i.e., new nesting material), which are known to activate VTA dopaminergic neurons. Therefore, we scattered the already built nest about the home environment of the test mice while performing time-locked fiber photometry, EEG-EMG and video recordings (Fig. 4h). We also introduced three glass marbles (novel objects) to the test mice following the nest scattering. We performed a detailed 1-s behavioral scoring of the videos and found that *Th+* VTA neurons showed low fluorescence and calcium transient rates during nest-building, compared to active waking

and novel object exploration (Fig. 4i–j). These findings suggest that sleep-related nest-building behavior naturally occurs under low dopaminergic tone.

Stimulation of *Th*$^+$ VTA neurons initiates wakefulness

We next examined the capacity of *Th*$^+$ VTA neurons to initiate and maintain wakefulness. While the chemogenetic approach is particularly suitable for carrying out prolonged inhibitions, it lacks the temporal resolution needed to study sleep-to-wake transitions. Therefore, we used optogenetics, which allows millisecond timescale precision, to study the effects of *Th*$^+$ VTA stimulation on wakefulness initiation and maintenance. We injected an AAV encoding channelrho-dopsin-2 (AAV5-DIO-EF1α-ChR2-eYFP, hereafter ChR2 mice; AAV5-DIO-EF1α-eYFP, hereafter eYFP mice, were used as controls) into the VTA of Th-Cre mice and implanted a fiber optic probe above the VTA and EEG-EMG electrodes (Fig. 5a,b). We examined the effect of photostimulation (5 s of photostimulation at 1 or 25 Hz) on sleep-to-wake transitions during the inactive, light phase. Phasic 25-Hz stimulation of *Th+* VTA neurons during NREM sleep induced an almost immediate transition to wakefulness in ChR2 but not in eYFP mice, even following 4 h of sleep deprivation (Fig. 5c,d and **Supplementary Fig. 5b**). In ChR2 mice the 25-Hz stimulation during NREM sleep induced a decrease in slow-wave activity (**Supplementary Fig. 5c**). Optogenetic stimulation of *Th+* VTA neurons at 1 or 25 Hz during REM sleep decreased REM episode duration in ChR2 mice compared with eYFP controls (Fig. 5e). Taken together, our findings demonstrate that *Th+* VTA neurons have a potent capacity to initiate wakefulness, even in the face of homeostatic sleep pressure.

Stimulation maintains wakefulness and inhibits nest-building

To investigate whether *Th*$^+$ VTA neurons can maintain wakefulness, we delivered optical stimuli at 25 Hz for 2 s min^{-1} during the first 6 h of the light phase (ZT 0–ZT 6; Fig. 6a). Semichronic stimulation of *Th*$^+$ VTA neurons was sufficient to induce almost continuous wakefulness and to inhibit both NREM and REM sleep during the entire 6 h of stimulation in ChR2 but not in eYFP mice (Fig. 6b – e). Moreover, optical stimulation produced a prominent 9-Hz theta component in the wake EEG power spectrum, which was present across all 6 h in ChR2 mice (**Supplementary Fig. 6d**). The NREM sleep EEG power spectrum in the first hour following termination of stimulation was noticeably different from the remaining hours of the light phase in ChR2 mice and contained a higher delta power (**Supplementary Fig. 6e**). During the following dark phase (ZT 12–ZT 0), the duration of wakefulness was significantly reduced and the duration of NREM and REM sleep was significantly increased in ChR2 mice (Fig. 6d,e). These rebound effects were similar to those observed following sleep deprivation by gentle handling during this circadian phase[31]. To validate the involvement of dopamine in the photostimulation-induced wakefulness, we pretreated mice with D1 and D2 receptor antagonists (SCH-23390 and eticlopride, respectively, 1 mg kg^{-1}, i.p., as in ref. 32), before the semichronic photostimulation. Dopamine receptor antagonism blocked the wake maintenance and sleep suppression induced by *Th*$^+$ VTA neurons stimulation (**Supplementary Fig. 6f**), indicating that dopamine signaling is key to this process.

To further investigate the causal role of *Th*$^+$ VTA neurons in nest-building behavior, we removed the old nest from the home environment of test mice just before the initiation of a semichronic photostimulation (2 s min^{-1}, from ZT 0–ZT 3), provided new nesting material and quantified nest-building 3 h later (Fig. 6f). Mice promptly rebuild a nest during the light phase if their old one is removed and new nesting material is provided. Control mice constructed nearly perfect nests during the test period, whereas ChR2 mice stimulated at 25 Hz left the nesting material practically untouched (Fig. 6g,h) despite being continuously awake. Taken together, these findings demonstrate that *Th*$^+$ VTA neurons are potent in maintaining electrocortical and behavioral wakefulness and that optically driven activity in these neurons is sufficient to suppress the motivation to engage in ethologically relevant sleep-related behavior.

Th$^+$ VTA neuron projections differentially modulate arousal

To elucidate the role of downstream targets of *Th*$^+$ VTA neurons in the modulation of sleep–wake states, we implanted a fiber optic probe above four output regions: the NAc, mPFC, central amygdala (CeA) and dorsal-lateral striatum (DLS) of Th-Cre mice following ChR2 and eYFP viral infusion into the VTA (AAV-DJ-DIO-EF1α-ChR2-eYFP or AAV-DJ-DIO-EF1α-eYFP; $n = 6$ per group for NAc and mPFC and 4 per group for CeA and DLS; Fig. 7a – d). Phasic photostimulation (25 Hz for 5 s) of the NAc, CeA and DLS projections in ChR2 mice during NREM sleep significantly reduced the latency to wake compared to that in eYFP mice and to 1-Hz stimulation ($P < 0.01$ for all three projections; Fig. 7e,g,h and **Supplementary Fig. 7a,c,d**). In contrast, photostimulation of the mPFC projections had no significant effect on NREM sleep duration (Fig. 7f and **Supplementary Fig. 7b**). During REM sleep, photostimulation of the NAc and DLS projections in ChR2 mice had no effect on REM duration (Fig. 7i,l and **Supplementary Fig. 7e,h**), whereas photostimulation of the mPFC and CeA projections reduced REM-to-wake latency compared with the control groups (Fig. 7j,k and **Supplementary Fig. 7f,g**).

To examine the capacity of *Th*$^+$ VTA projections to maintain wake-fulness, we delivered optical stimuli (25 Hz for 2 s min^{-1}) during the first 6 h of the light phase (ZT 0–ZT 6; Fig. 7m–x). The only projection capable of maintaining arousal was the NAc, and semichronic stimulation of this circuit increased wakefulness and decreased NREM and REM sleep (Fig. 7m,q,u) but to a lesser extent than optically activating *Th*$^+$ VTA cell bodies (Fig. 6d). Semichronic stimulation of all other projections had no significant effect on sleep–wake architecture (P(interaction) > 0.2 for all projections; Fig. 6n–p,r–t,v–x). Interestingly, semichronic stimulation of either of the terminals did not prevent the construction of a new nest (**Supplementary Fig. 7i–l**), in contrast to *Th*$^+$ VTA cell body stimulation (Fig. 6h). Together our findings suggest that different projections of *Th*$^+$ VTA neurons differentially modulate arousal, but most of the examined effects on sleep–wake states are mediated by the NAc projections.

DISCUSSION

To uncover the causal role of VTA dopaminergic neurons in sleep–wake regulation, we combined fiber photometry, behavioral, chemogenetic, optogenetic and polysomnographic

methods with spatial and temporal resolutions relevant to natural sleep–wake events. We demonstrate a causal role for VTA dopaminergic neurons in the regulation of sleep–wake states and sleep-related behaviors. We reveal arousal state-dependent alteration in neuronal activity of VTA dopaminergic neurons, identifying a reduction in population activity during NREM sleep. We show that VTA dopaminergic neurons are capable of maintaining long-term wakefulness during a period of high sleep pressure and are necessary for the maintenance of wakefulness even during a period of low sleep pressure. We further show that even in arousal-promoting environments VTA dopaminergic neurons are necessary for the maintenance of wakefulness. We begin to establish a circuit through which VTA dopaminergic neurons regulate arousal and demonstrate that the NAc pathway promotes wakefulness and suppresses sleep. Finally, we uncover a fundamental role for VTA dopaminergic neurons in the regulation of goal-directed and sleep-related nesting behavior. To the best of our knowledge, this is the first demonstration of a causal regulation of sleep-related nest-building by a specific neuronal population.

Pharmacological agents targeting dopamine-signaling pathways can potently modulate wakefulness[13,19], and genetically modified animal models lacking different components of dopamine-signaling pathways (for example, dopamine transporters and dopamine receptors) also clearly implicate dopamine in sleep–wake regulation[14,15,17–19,32], yet the neuronal sources of dopamine in this regard have thus far been unclear. Early lesioning and electrophysiological studies[8,9,11,12] led to the influential hypothesis that VTA dopaminergic neurons are not involved in the regulation of sleep–wake states[6,7], and one neuronal population hypothesized to mediate the effects of dopamine on arousal was the group of ventral periaqueductal gray matter (vPAG) dopaminergic neurons[7,33]. vPAG dopaminergic neurons show c-Fos immunoreactivity during wakefulness but not during sleep, and lesioning these neurons reduces wakefulness and increases sleep[34]. We now show that VTA dopaminergic neurons not only display arousal-state-dependent alterations in population activity but potently and bidirectionally regulate sleep–wake states. We demonstrate that VTA dopaminergic neurons are necessary for arousal and that their chemogenetic inhibition suppresses wakefulness to promote both NREM and REM sleep, whereas optogenetic stimulation promotes long-term wakefulness and suppresses sleep. Future studies may uncover the functional relationship between vPAG and VTA dopaminergic populations in sleep–wake regulation and reveal whether they act in concert or in independent pathways to generate and maintain arousal.

Our findings strongly indicate that the sleep induced by inhibition of VTA dopaminergic neurons is physiological. Following chemogenetic inhibition mice show polysomnographic characteristics of sleep, reduced muscular activity and typical EEG power spectrum for each sleep state. In addition, before inducing sleep, chemogenetic inhibition of VTA dopaminergic neurons promotes nest-building, a sleep-preparatory behavior. We further demonstrate that activity in VTA dopaminergic neurons is relatively low during experimentally induced nest-building, and optogenetic activation suppresses this behavior. Interestingly, nest-building in zebra finches (*Taeniopygia guttata*) is also correlated with reduced VTA dopaminergic activity[35]. (Although zebra finches sleep in their nests, they also rear their young there, and this study was not performed in the context of sleep.) These findings suggest that sleep and sleep-related behaviors are normally displayed in a state of

reduced VTA dopaminergic tone. Our study proposes an active role for VTA dopaminergic neurons in the maintenance of the behavioral and electrocortical wake state and places VTA dopaminergic neurons at a crucial node in the sleep–wake circuitry. The observed increase in REM sleep following the inhibition of VTA dopaminergic neurons was unexpected in light of our (and previous)[23] findings of increased activity in these neurons during REM sleep. Further investigations may uncover whether activity in functionally distinct subpopulations of VTA dopaminergic neurons is associated with REM initiation and maintenance.

The capacity to increase wakefulness in response to specific environmental conditions and homeostatic needs is essential for survival in nature. Strong behavioral and electrocortical arousal are required for motivated behaviors, such as mating, food-seeking and predator confrontation. VTA dopaminergic neurons are well placed to integrate motivational information for the allocation of suitable levels of arousal for behavioral performance, yet their causal role in electrocortical wake generation had not been thoroughly explored. Among the known neuronal populations that contribute to the awake state and act in concert to generate and maintain arousal are the noradrenergic locus coeruleus, histaminergic tuberomammillary nucleus, cholinergic basal forebrain and hypocretinergic lateral hypothalamus neurons[6,7]. It is thus notable that inhibition of VTA dopaminergic neurons is sufficient to prevent arousal in the face of some of the most salient stimuli for animals, related to reproduction, feeding and predation. Relating our findings to previous work linking dopamine to motivation[4,5], our results suggest that VTA dopaminergic inhibition not only hampers the motivation to properly attend to salient stimuli but also lessens the motivation to stay awake. Yet, following VTA dopaminergic inhibition, mice do engage in complex goal-directed and sleep-related nest-building behavior, suggesting that in parallel with the reduced wake motivation, the motivation to sleep and to engage in sleep-related behaviors is increased. It has been suggested that the NAc participates in the regulation of sleep–wake states[36,37], and our findings that photostimulation of VTA–NAc projections initiate and maintain wakefulness support this premise and begin to establish the circuit through which VTA dopaminergic neurons regulate sleep–wake states. Taken together, our findings suggest that VTA dopaminergic neurons are a critical link between motivational processes and sleep–wake regulation and implicate VTA dopaminergic neurons as key mediators of adaptive salience-induced arousal. It is also notable that dopamine is a major regulator of sleep–wake states in insects[38–40], which could suggest an ancient origin for dopamine in arousal regulation.

A large body of literature has demonstrated that VTA dopaminergic neurons have essential roles in motivation, reward-seeking and reinforcement learning[1–5,41]. In addition, optogenetic and chemogenetic tools are frequently used to activate and inhibit these neurons[24,42–46]. However, few studies have examined dopamine-related behaviors over longer timescales, as we have done here. Our findings that VTA dopaminergic neurons can potently and bidirectionally regulate arousal have, therefore, far-reaching implications outside the field of sleep research and emphasize the importance of considering arousal influences in experimental designs.

Several neuropsychiatric disorders, including major depressive and bipolar disorders, schizophrenia and substance abuse, are accompanied by dysregulation of dopamine

signaling pathways and the sleep–wake cycle[47–50], yet relatively little is known about their mechanistic relationship. It is hypothesized that many comorbid pathologies found in these neuropsychiatric disorders arise from a destabilization of sleep–wake mechanisms[48]. Our findings suggest a mechanistic framework for this association and reveal opportunities for investigations on dopamine-related sleep–wake dysregulation in neuropsychiatric disorders.

ONLINE METHODS

Mice

Tyrosine hydroxylase knock-in mice (Th-IRES-Cre; EM:00254) were obtained from the European Mouse Mutant Archive and backcrossed to C57BL/6J wild-type mice for >15 generations. We used only male heterozygous mice, aged 8–10 weeks at the start of experimental procedures. During all sleep and behavioral experimentations, mice were housed in individual Plexiglas recording chambers at constant temperature (23 ± 1 °C), humidity (40–60%) and circadian cycle (12 h light-dark cycle; lights on (ZT 0) at 7:00 a.m.). Food and water were available *ad libitum*. All experiments were performed in accordance with the guidelines described in the US National Institutes of Health Guide for the Care and Use of Laboratory Animals and were approved by Stanford University's Administrative Panel on Laboratory Animal Care.

Virus preparation

Cre-inducible recombinant AAV vectors carrying chemogenetic (AAV-EF1α-DIO-hM4Di-mCherry and AAV-EF1α-DIO-mCherry) and optogenetic (AAV-EF1α-DIO-ChR2(H134R)-eYFP and AAV-EF1α-DIO-eYFP) transgenes were serotyped with AAV5 coat proteins and packaged by the viral vector core at the University of North Carolina. The final viral concentration of the chemogenetic transgenes were 5×10^{12} genome copies (gc) ml^{-1} and the optogenetic transgene were 2×10^{12} gc ml^{-1}. The transgenes for fiber photometry (AAV-EF1α-DIO-GCaMP6f and AAV-EF1α-DIO-GFP) and optogenetic terminal stimulations (AAV-EF1α-DIO-ChR2(H134R)-eYFP and AAV-EF1α-DIO-eYFP) were serotyped with AAV-DJ coat proteins and packaged by the viral vector core at Stanford University. The final viral concentrations were 1.1×10^{13} and 5.8×10^{13} gc ml^{-1}, respectively. Aliquots of virus were stored at −80 °C before stereotaxic injection.

Surgery

At the start of surgical procedures, mice were anesthetized with ketamine and xylazine (100 and 20 mg kg^{-1}, respectively; intraperitoneal injection, i.p.) and placed on a stereotaxic frame (David Kopf Instruments, Tujunga, CA, USA). To selectively express the viral constructs in dopaminergic neurons of the VTA, we infused recombinant AAV unilaterally to the VTA (AP = −3.3 mm; ML = 0.2 mm; DV = −4.5 mm) of Th-IRES-Cre mice. The virus was injected through a stainless steel 33-gauge internal cannula (Plastics One, Inc., Roanoke, VA) attached to a 10 μl Hamilton syringe, at a rate of 0.05–0.1 μl min^{-1} (1 μl total volume in chemogenetic and optogenetic cell body experiments and 0.4 μl of the AAV-DJ viruses in fiber photometry and optogenetic terminal stimulation experiments). After infusion, the cannula was kept at the injection site for at least 8 min and then slowly withdrawn. After injections, mice were implanted with two gold-plated miniature screw

electrodes (AP = 1.5 mm, ML = −1.5 mm and AP = −3.5 mm, ML = −2.8 mm) and two EMG wire electrodes (316SS/44T, Medwire), previously soldered to a four-pin connector. The EMG electrodes were inserted between the neck musculature. The EEG-EMG device was affixed to the skull with C&B Metabond (Parkell) and dental acrylic. Mice used for fiber photometry and optogenetic experiments also received surgical implantation of a monofiberoptic cannula (400 μm and 200 μm, respectively; Doric Lenses, Inc., Quebec, Canada), above the VTA (AP = −3.3 mm; ML = 0.2 mm; DV = −4.3 mm), NAc (AP = 1.1 mm; ML = 1 mm; DV = −3.8 mm), mPFC (AP = 1.7 mm; ML = 0.35 mm; DV = −1.45 mm), CeA (AP = −1.4 mm; ML = 2.68 mm; DV = −4.15 mm) or DLS (AP = 0.5 mm; ML = 2 mm; DV = −2.9 mm). We used surgical sutures to close the skin, and the mouse was kept in a warm environment until resuming normal activity. Mice were allowed to recover for 3 weeks, and then acclimated to a flexible EEG-EMG connection cable and an optical patch cord (in fiber photometry and optogenetic experiments) for ~10 d within individual recording chambers. Each cable was flexible so that mice could freely move about their cages. We found that 79 ± 1.2% of hM4Di cells in the VTA co-expressed TH ($n = 4$ mice).

Fiber photometry recordings

Fiber photometry recordings were performed similarly to those in ref. 25. Briefly, we sinusoidally modulated blue light from a 470-nm excitation LED (M470F3, Thorlabs, NJ, USA) at 211 Hz, using a custom Matlab program (MathWorks, Natick, MA, USA) and a multifunction data acquisition device (NI USB-6259, National Instruments, Austin, TX, USA). The blue light was passed through a GFP excitation filter (MF469-35, Thorlabs), reflected off a dichroic mirror (MD498, Thorlabs), and coupled using a fiber collimation package (F240FC-A, Thorlabs) into a low-fluorescence patch cord (400 μm, 0.48 NA; Doric Lenses) connected to the implanted optic fiber (400 μm, 0.48 NA; Doric Lenses) by a zirconia sleeve (Doric Lenses). GCaMP6f fluorescence was collected through the excitation patch cord, passed through a GFP emission filter (MF525-39, Thorlabs), and focused onto a photodetector (Model 2151, Newport, Irvine, CA, USA) using a lens (LA1540-A, Thorlabs). The signal was sent to a lock-in amplifier (30-ms time constant, Model SR830, Stanford Research Systems, Sunnyvale, CA, USA) that was synchronized to 211 Hz. Signals from the amplifiers were collected at 1 KHz using a custom Matlab program and a multifunction data acquisition device (National Instruments).

Fiber photometry data analysis

The photometry signal was down-sampled using interpolation to match the EEG and EMG sampling rate of 256 Hz (see below). For each experiment, the photometry signal F was converted to $\Delta F/F$ by

$$\Delta F/F(t) = \frac{F(t) - \text{median}(F)}{\text{median}(F)}$$

In a minority of sessions, the photometry signal showed a short decay at the beginning of the recording. To address this in a general way across all sessions, the $\Delta F/F$ signal from each session was fitted with a decreasing exponential of the form $a \times e^{bx}$, where $a > 0$ and $b < 0$.

We then subtracted the exponential fit from the original Δ*F/F* signal. This procedure corrected the signal decrease when it occurred and left the signal unchanged when no decrease was observed. We detected transients similar to those reported by previous studies[24] (**Supplementary Fig. 1 a – g**). Briefly, we generated two filtered Δ*F/F* signals, one low-pass filtered at 0–4 Hz, and the other low-pass filtered at 0–40 Hz. We calculated a trace of the derivative of their squared difference and identified candidate transient times by thresholding this signal at mean + 2 s.d. We further required that candidate transient times be during high Δ*F/F* times by thresholding at mean + 2 s.d. Lastly, the exact peak time of each transient was identified by taking the maximal value of the thresholded signal within each transient. For each session and for each arousal state, we calculated the following calcium transient measures: (i) mean transient rate, (ii) mean transient amplitude and (iii) mean transient amplitude × amplitude rate.

For the sleep–wake analysis (Fig. 1 and **Supplementary Fig. 1**), we recorded data during 8 sessions per mouse, each 10–45 min long. We only used sessions during which mice showed all three arousal states (wake, NREM sleep and REM sleep). For each session we calculated the mean Δ*F/F* during all times of wake, NREM sleep and REM sleep. For the state transition analyses, we identified all time points of state transition and aligned Δ*F/F* around these times (± 50 s). Transition-aligned Δ*F/F* traces were Gaussian smoothed (sigma = 3 s).

For the salient stimuli presentation (Fig. 3a), we recorded data for 5 min, once for each mouse ($n = 4$). For the nest-building behavior experiment (Fig. 4h – j), we recorded data for 45 min once for each mouse ($n = 4$).

Polysomnographic recording and analysis

EEG and EMG signals derived from the surgically implanted electrodes were amplified (Grass Technologies) and digitized at 256 Hz using sleep recording software (Vital Recorder, Kissei Comtec America). Using sleep analysis software (SleepSign for Animal, Kissei Comtec America) we digitally filtered the signal (EEG: 0.3–25 Hz, EMG: 25–50 Hz) and spectrally analyzed it by fast Fourier transformation. The recordings were first scored semiautomatically by 4-s epochs for wake, NREM sleep and REM sleep. The scoring was next inspected visually based on the EEG-EMG waveforms and power spectra and corrected when appropriate. All scoring was done by an investigator (A.E.-R.) blind to the viral transgene delivered to the animal and to the experimental manipulation. Wakefulness was defined as desynchronized low-amplitude EEG and heightened tonic EMG activity with phasic bursts. NREM sleep was defined as synchronized, high-amplitude, low-frequency (0.5–4 Hz) EEG and substantially reduced EMG activity compared with wakefulness, with no phasic bursts. REM sleep was defined as having a pronounced theta rhythm (4–9 Hz) with no EMG activity. The EEG power spectrum data (Fig. 2h and **Supplementary Fig. 4a,b** and **6c,d,e**) are expressed as relative values to the total power of the same stage. For the change in delta power with time analysis (**Supplementary Fig. 3c**) we used episodes lasting ≥60 s and examined the correlation for the first 60 s of NREM sleep. We omitted one hM4Di mouse from the spectrogram presented in Figure 2f – g because he showed < 1% REM sleep following saline injection.

Salient stimuli presentation

Test mice, individually housed and connected to an EEG-EMG recording cable, were injected during the dark phase (ZT 13.75) with either saline or CNO (1 mg kg^{-1}). Forty-five minutes later, a stimulus was placed in their home cage, for a period of 1 h. EEG-EMG signals were continuously recorded from the test mice during this period. In each experimental session, each test mouse was exposed to one stimulus following either saline or CNO injection. Half of the mice were first treated with saline, while the other half first with CNO. We performed different experiments at least 1 week apart.

In experiments in which salient stimuli were inaccessible, we placed each stimulus on a petri dish lid and covered it by an inverted cylindrical wire grating (11 cm in height, bottom diameter 10.5 cm, bars spaced 1 cm apart; Galaxy Cup, Spectrum Diversified Designs, Inc., Streetsboro, OH, USA) before the placement in the test mice cages. A weighted glass beaker was placed on top of the wire cylinder to prevent test mice from climbing it. In the experiment with the high-fat chow (see below), an additional paper tube punctuated with small holes was placed between the chow and the wire cylinder; to prevent test mice from consuming the chow.

We used three salient stimuli: (i) 8-week-old female C57BL/6J mice (Jackson Laboratory); (ii) high-fat chow (D12451, Research Diets, Inc.); and (iii) 10 μl of 2,3,5-trimethyl-3-thiazoline, a component of fox odor (TMT, #300000368; Contech Enterprises Inc., Canada) applied to filter paper. Test mice were habituated for 5 d to the presence of an empty wire cylinder in their home cage (1 h d^{-1}). Female mice were habituated for 5 d to handling and to the placement in a wire cylinder (30 min d^{-1}). Each female participated in only one experimental session (i.e., a single exposure to one test mouse). We provided test mice with a small piece (0.3 g) of high-fat chow during the two days preceding the high-fat chow experiment.

In each experimental session, we video recorded one mouse using a Panasonic Lumix DMC-ZS7 camera. The speed of the videos was accelerated ×16 or ×64, as indicated.

Food deprivation

16 h before the compound injection (at ZT 22) we removed all pieces of food from the home cage environment of the mice.

Nest-building behavior

In the chemogenetic experiment presented in Figure 4a–d, we injected mice with either saline or CNO (1 mg kg^{-1}) during the dark phase (ZT 13.75). Forty-five minutes after the injections, we transferred the test mice to new individual cages containing 3 g pressed cotton squares (1–1.5 squares, to match 3 g precisely; Nestlet, Ancare, UK agent, Lillico). We evaluated nest-building 1 h later. Each mouse was tested following both saline and CNO injection, at least 1 week apart. Half of the mice were treated first with saline and the other with CNO.

In the optogenetic experiment (Fig. 6f – h and **Supplementary Fig. 7i – l**), just before the beginning of the photostimulation (ZT 0) we removed the nest (i.e., all pieces of cotton) from the home cage of the test mice. Upon the start of photostimulation we placed a new 3 g Nestlet in the home cages of the test mice. We evaluated nest-building 3 h later (at ZT 3).

We evaluated nest building, as in ref. 51, using a five-point scale:

1. Nestlet not noticeably touched (>90% intact).
2. Nestlet partially torn up (50–90% remaining intact).
3. Nestlet mostly shredded but with no identifable nest site; i.e., the cotton is not gathered into a nest but spread around the cage (<50% of the Nestlet remains intact, but <90% is within a quarter of the cage floor area).
4. An identifable but flat nest (>90% of the Nestlet is torn up). The material is gathered into a nest within a quarter of the cage floor area, with walls higher than mouse body height (of a mouse curled up on its side) for less than 50% of its circumference.
5. A perfect or near-perfect nest (>90% of the Nestlet is torn up). The nest is a crater, with walls higher than mouse body height for more than 50% of its circumference.

For analysis, we used the nonparametric Wilcoxon matched-pairs signed rank test, as in ref. 51.

In the chemogenetic experiment presented in Figure 4h – j we used shredded paper as nesting material, since it enabled the transfer of nests without altering their shape; nests made solely from cotton are easily damaged by handling.

Fiber photometry during nest-building

We scattered the already built nest about the home environment of test mice while performing time-locked fiber photometry, EEG-EMG and video recordings. We also introduced three glass marbles (novel objects) to the test mice home cage after scattering the nest. We video recorded mice using a Panasonic Lumix DMC-ZS7 camera and performed a detailed 1-s behavioral scoring of the videos off-line. Novel object' was defined as a direct contact between the test mouse and a marble. Active waking was defined as a state in which the test mouse was awake and alert, but not engaging in grooming, nest-building or novel object exploration. 'Nest-building' was assigned to mice engaging in pulling, carrying, fraying, push-digging, sorting and fluffing of nesting material and bedding, as previously described[30]. For the comparison of mean fluorescence we used data from all 1-s epochs in four experimental mice ('novel object' $n = 374$; 'active waking' $n = 2{,}801$; 'nest-building' $n = 2{,}143$). For the comparison of mean transient rate, we used mean values per mice ($n = 4$).

Core body temperature measurement

Body temperature was recorded, at the beginning of the light phase, with a lubricated rectal probe connected to digital thermometer (BAT-12 Microprobe-Thermometer; Physitemp; NJ,

USA) 15, 30, 60, 120 and 240 min following CNO (1 mg kg^{-1}) administration in mCherry and hM4Di mice.

Photostimulation

Three weeks after viral infection and implantation, mice were connected to fiber optic patch cords (Doric Lenses) using zirconia sleeves (Doric Lenses). Mice were allowed to habituate to the patch cords for 7–10 d. All optogenetic stimulations (15 ms pulses at 1 and 25 Hz; see text) were generated by a waveform generator (Master-8; AMPI, Jerusalem, Israel) that triggered blue-light lasers (473 nm; LaserGlow). We adjusted the light power of the lasers such that the light power exiting the optic fiber was 20 mW In acute photostimulation experiments, we monitored EEG-EMG signals in real time in order to precisely time the delivery of optical stimuli (5 s at 1 or 25 Hz) at the onset of NREM or REM epochs (~10 s from onset).

Sleep deprivation

Mice were sleep deprived for 4 h by gentle handling. Mice were continuously observed by an experimenter (A.E.-R.) and their EEG-EMG signal was recorded. If an animal remained motionless for a few seconds, he was gently touched with a soft brush. This method of sleep deprivation has been shown not to increase plasma corticosterone or adrenocorticotropic hormone levels, suggesting that this procedure does not produce significant stress in mice[52].

Pharmacological injections

Pharmacological compounds were prepared in sterile 0.9% saline. All compounds were administered i.p. Compounds included: CNO (1 mg kg^{-1}, Enzo Life Sciences, Inc.), D1-antagonist (1 mg kg^{-1}; Sigma-Aldrich, SCH-23390 hydrochloride) and D2-antagonist (1 mg kg^{-1}; Sigma-Aldrich, eticlopride hydrochloride).

Histology

Mice were anesthetized with ketamine and xylazine (100 and 20 mg kg^{-1}, respectively, i.p.) and perfused transcardially with 1× PBS, followed by 4% paraformaldehyde in PBS. Brains were extracted, postfixed overnight at 4 °C, and cryoprotected in 30% sucrose dissolved in 1× PBS containing 0.1% NaN_3 for 48 h at 4 °C. Brains were sectioned at 30 μm on a cryostat (Leica Microsystems), collected in PBS containing 0.1% NaN_3 and stored at 4 °C. Sections underwent immunohistochemical staining as described below. Primary antibodies were used at 1:2,000 dilution: chicken anti-tyrosine hydroxylase (#TYH, Aves Labs, Inc.) and rabbit anti-Fos (#sc-52, Santa Cruz). Immunofluorescent secondary antibodies were used at 1:500 dilution: donkey anti-chicken Alexa Fluor 488 (#703-545-155, Jackson ImmunoResearch Laboratori;es, Inc.) for mCherry and TH colocalization, and donkey anti-chicken CF350 (#20275, Biotium) plus donkey anti-rabbit Alexa Fluor 488 (#711-545-152, Jackson ImmunoResearch Laboratories, Inc.) for c-Fos and TH double-labeling.

For immunofluorescence staining, brain sections were washed in PBS for 5 min and then incubated in a blocking solution composed of PBS with 0.3% Triton X-100 (PBST) containing 4% bovine serum albumin for 1 h. Sections were then incubated for ~16 h in block solution containing primary antibodies. After three 5-min washes in PBS, sections

were incubated in blocking solution for 1 h and then incubated for 2 h in blocking solution containing secondary antibodies. Sections were washed three times for 5 min each in PBS, mounted onto SuperFrost Plus glass slides (VWR, #48311-703) and coverslipped with Vectashield containing DAPI Mounting Media (Vector Laboratories, #H-1200).

Microscopy and image analysis

Images for mCherry and TH colocalization were collected on a Zeiss LSM710 inverted confocal microscope and generated with ZEN software (Zeiss). Images for c-Fos protein and TH analyses were collected on a Zeiss Axioimager M1 wide-field fluorescent microscope using reflected light (immunofluorescence staining). Digital images were minimally processed using ImageJ (NIH) to enhance brightness and contrast for optimal representation. All digital images were processed in parallel, with experimenters blind to the viral transduction.

All immunohistochemical analyses were performed on serial sections from $n = 4$ mice per group. For mCherry and TH colocalization analyses, mCherry-positive neurons in the VTA were scored for presence of TH (3 sections per mouse; −2.90 to −3.60 mm from bregma). For c-Fos protein and TH double-labeling analyses, TH-positive neurons in midline cell groups from hypothalamus to hindbrain were scored for the presence of c-Fos protein (18 sections per mouse, −1.6 to −4.4 mm from bregma). All ChR2 vs. eYFP analyses were performed by investigators blind to the viral transduction.

Statistics

Sample sizes were chosen based upon previous publications using optogenetic and chemogenetic tools for the study of the sleep–wake circuitry[53–55]. Data distribution was assumed to be normal but this was not formally tested. Mice were removed from analysis if no viral expression was found ($n = 4$). We used two-way RM ANOVAs for analyses of latencies, durations, calcium signal and EEG power spectrograms across arousal states (Figs. 1d,e, Fig. 2d,h –k, 3b–h, 4b,f, 5d,e, 6d,e and 7e–x). We used Wilcoxon matched-pairs signed rank tests for the analysis of nest-building behavior (Figs. 4d and 6h). We used two-way ANOVAs for the analysis of fluorescence across behavioral states and one-way ANOVAs for transient rate analysis (Fig. 4i,j, respectively). We analyzed all data using Prism 6.0 (GraphPad Software) except for fluorescence and transient rates following nest destruction (Fig. 4i–j), which were analyzed using Matlab R2015a software. Data are presented as mean ± s.e.m. unless otherwise indicated. For the preparation of the figures, we used Matlab R2008b, Matlab R2015a and Prism 6.0 and then exported the data into Adobe Illustrator CS6 (Adobe Systems).

A **Supplementary Methods Checklist** is available.

Data availability

The data that support the findings of this study are available from the corresponding author upon reasonable request.

Code availability

Data analyses were conducted in Matlab using scripts available from the corresponding author upon reasonable request.

Acknowledgments

We thank T. Davidson for assistance in the set-up of the fiber photometry rig, A. Whittle for assistance in core body temperature measurements and for feedback on the manuscript, A. Rolls and P. Bonnavion for early training in sleep–wake recording and viral manipulations and discussion and J. Garner for discussion. This work was supported by National Institutes of Health (NIH) grants RO1-MH087592, RO1-MH102638 and RO1-AG04767 (L.d.L.), a Brain and Behavior Research Foundation (NARSAD) grant (L.d.L.), the US Israel Binational Science Foundation and the Klarman Family Foundation (L.d.L.), Edmond and Lily Safra Center of Brain Science (ELSC) postdoctoral fellowships (A.E.-R.) and NIH F32 AA022832 (W.J.G.). We thank the Stanford Neuroscience Microscopy Service, supported by NIH NS069375.

References

1. Robbins TW, Everitt BJ. A role for mesencephalic dopamine in activation: commentary on Berridge (2006). Psychopharmacology (Berl.). 2007; 191:433–437. [PubMed: 16977476]
2. Berridge KC, Robinson TE. What is the role of dopamine in reward: hedonic impact, reward learning, or incentive salience. Brain Res. Brain Res. Rev. 1998; 28:309–369. [PubMed: 9858756]
3. Salamone JD, Correa M. The mysterious motivational functions of mesolimbic dopamine. Neuron. 2012; 76:470–485. [PubMed: 23141060]
4. Wise RA. Dopamine, learning and motivation. Nat. Rev. Neurosci. 2004; 5:483–494. [PubMed: 15152198]
5. Schultz W. Multiple dopamine functions at different time courses. Annu. Rev. Neurosci. 2007; 30:259–288. [PubMed: 17600522]
6. España RA, Scammell TE. Sleep neurobiology from a clinical perspective. Sleep. 2011; 34:845–858. [PubMed: 21731134]
7. Saper CB, Fuller PM, Pedersen NP, Lu J, Scammell TE. Sleep state switching. Neuron. 2010; 68:1023–1042. [PubMed: 21172606]
8. Steinfels GF, Heym J, Strecker RE, Jacobs BL. Behavioral correlates of dopaminergic unit activity in freely moving cats. Brain Res. 1983; 258:217–228. [PubMed: 6824912]
9. Trulson ME, Preussler DW. Dopamine-containing ventral tegmental area neurons in freely moving cats: activity during the sleep-waking cycle and effects of stress. Exp. Neurol. 1984; 83:367–377. [PubMed: 6692873]
10. Trulson ME, Preussler DW, Howell GA. Activity of substantia nigra units across the sleep-waking cycle in freely moving cats. Neurosci. Lett. 1981; 26:183–188. [PubMed: 7301205]
11. Miller JD, Farber J, Gatz P, Roffwarg H, German DC. Activity of mesencephalic dopamine and non-dopamine neurons across stages of sleep and walking in the rat. Brain Res. 1983; 273:133–141. [PubMed: 6616218]
12. Jones BE, Bobillier P, Pin C, Jouvet M. The effect of lesions of catecholamine-containing neurons upon monoamine content of the brain and EEG and behavioral waking in the cat. Brain Res. 1973; 58:157–177. [PubMed: 4581335]
13. Boutrel B, Koob GF. What keeps us awake: the neuropharmacology of stimulants and wakefulness-promoting medications. Sleep. 2004; 27:1181–1194. [PubMed: 15532213]
14. Wisor JP, et al. Dopaminergic role in stimulant-induced wakefulness. J. Neurosci. 2001; 21:1787–1794. [PubMed: 11222668]
15. Qu WM, Huang ZL, Xu XH, Matsumoto N, Urade Y. Dopaminergic D1 and D2 receptors are essential for the arousal effect of modafinil. J. Neurosci. 2008; 28:8462–8469. [PubMed: 18716204]
16. Holst SC, et al. Dopaminergic role in regulating neurophysiological markers of sleep homeostasis in humans. J. Neurosci. 2014; 34:566–573. [PubMed: 24403155]

17. Dzirasa K, et al. Dopaminergic control of sleep-wake states. J. Neurosci. 2006; 26:10577–10589. [PubMed: 17035544]
18. Qu WM, et al. Essential role of dopamine D2 receptor in the maintenance of wakefulness, but not in homeostatic regulation of sleep, in mice. J. Neurosci. 2010; 30:4382–4389. [PubMed: 20335474]
19. Monti JM, Monti D. The involvement of dopamine in the modulation of sleep and waking. Sleep Med. Rev. 2007; 11:113–133. [PubMed: 17275369]
20. Zhou QY, Palmiter RD. Dopamine-deficient mice are severely hypoactive, adipsic, and aphagic. Cell. 1995; 83:1197–1209. [PubMed: 8548806]
21. Ungerstedt U. Adipsia and aphagia after 6-hydroxydopamine induced degeneration of the nigro-striatal dopamine system. Acta Physiol. Scand. Suppl. 1971; 367:95–122. [PubMed: 4332694]
22. Léna I, et al. Variations in extracellular levels of dopamine, noradrenaline, glutamate, and aspartate across the sleep--wake cycle in the medial prefrontal cortex and nucleus accumbens of freely moving rats. J. Neurosci. Res. 2005; 81:891–899. [PubMed: 16041801]
23. Dahan L, et al. Prominent burst firing of dopaminergic neurons in the ventral tegmental area during paradoxical sleep. Neuropsychopharmacology. 2007; 32:1232–1241. [PubMed: 17151599]
24. Gunaydin LA, et al. Natural neural projection dynamics underlying social behavior. Cell. 2014; 157:1535–1551. [PubMed: 24949967]
25. Lerner TN, et al. Intact-brain analyses reveal distinct information carried by SNc dopamine subcircuits. Cell. 2015; 162:635–647. [PubMed: 26232229]
26. Alexander GM, et al. Remote control of neuronal activity in transgenic mice expressing evolved G protein-coupled receptors. Neuron. 2009; 63:27–39. [PubMed: 19607790]
27. Hediger H. Comparative observations on sleep. Proc. R. Soc. Med. 1969; 62:153–156. [PubMed: 5775231]
28. Meddis R. On the function of sleep. Anim. Behav. 1975; 23:676–691. [PubMed: 169715]
29. Moruzzi G. Sleep and instinctive behavior. Arch. Ital. Biol. 1969; 107:175–216. [PubMed: 4311356]
30. Gaskill BN, et al. Heat or insulation: behavioral titration of mouse preference for warmth or access to a nest. PLoS One. 2012; 7:e32799. [PubMed: 22479340]
31. Curie T, et al. Homeostatic and circadian contribution to EEG and molecular state variables of sleep regulation. Sleep. 2013; 36:311–323. [PubMed: 23450268]
32. Burgess CR, Tse G, Gillis L, Peever JH. Dopaminergic regulation of sleep and cataplexy in a murine model of narcolepsy. Sleep. 2010; 33:1295–1304. [PubMed: 21061851]
33. Brown RE, Basheer R, McKenna JT, Strecker RE, McCarley RW. Control of sleep and wakefulness. Physiol. Rev. 2012; 92:1087–1187. [PubMed: 22811426]
34. Lu J, Jhou TC, Saper CB. Identification of wake-active dopaminergic neurons in the ventral periaqueductal gray matter. J. Neurosci. 2006; 26:193–202. [PubMed: 16399687]
35. Hall ZJ, Healy SD, Meddle SL. A role for nonapeptides and dopamine in nest-building behaviour. J. Neuroendocrinol. 2015; 27:158–165. [PubMed: 25514990]
36. Lazarus M, Chen JF, Urade Y, Huang ZL. Role of the basal ganglia in the control of sleep and wakefulness. Curr. Opin. Neurobiol. 2013; 23:780–785. [PubMed: 23465424]
37. Qiu MH, et al. The role of nucleus accumbens core shell in sleep-wake regulation their involvement in modafinil-induced arousal. PLoS One. 2012; 7:e45471. [PubMed: 23029032]
38. Andretic R, van Swinderen B, Greenspan RJ. Dopaminergic modulation of arousal in Drosophila. Curr. Biol. 2005; 15:1165–1175. [PubMed: 16005288]
39. Kume K, Kume S, Park SK, Hirsh J, Jackson FR. Dopamine is a regulator of arousal in the fruit fly. J. Neurosci. 2005; 25:7377–7384. [PubMed: 16093388]
40. Pimentel, D., et al. Operation of a homeostatic sleep switch. Nature. 2016. http://dx.doi.org/10.1038/nature19055
41. Salamone JD, Cousins MS, Snyder BJ. Behavioral functions of nucleus accumbens dopamine: empirical conceptual problems with the anhedonia hypothesis. Neurosci. Biobehav. Rev. 1997; 21:341–359. [PubMed: 9168269]

42. Zhang, F., et al. Optogenetics in freely moving mammals: dopamine and reward. Cold Spring Harb. Protoc. 2015. http://dx.doi.org/10.1101/pdb.top086330
43. Adamantidis AR, et al. Optogenetic interrogation of dopaminergic modulation of the multiple phases of reward-seeking behavior. J. Neurosci. 2011; 31:10829–10835. [PubMed: 21795535]
44. Tye KM, et al. Dopamine neurons modulate neural encoding and expression of depression-related behaviour. Nature. 2013; 493:537–541. [PubMed: 23235822]
45. Chaudhury D, et al. Rapid regulation of depression-related behaviours by control of midbrain dopamine neurons. Nature. 2013; 493:532–536. [PubMed: 23235832]
46. Danjo T, Yoshimi K, Funabiki K, Yawata S, Nakanishi S. Aversive behavior induced by optogenetic inactivation of ventral tegmental area dopamine neurons is mediated by dopamine D2 receptors in the nucleus accumbens. Proc. Natl. Acad. Sci. USA. 2014; 111:6455–6460. [PubMed: 24737889]
47. Cousins DA, Butts K, Young AH. The role of dopamine in bipolar disorder. Bipolar Disord. 2009; 11:787–806. [PubMed: 19922550]
48. Wulff K, Gatti S, Wettstein JG, Foster RG. Sleep and circadian rhythm disruption in psychiatric and neurodegenerative disease. Nat. Rev. Neurosci. 2010; 11:589–599. [PubMed: 20631712]
49. Parekh PK, Ozburn AR, McClung CA. Circadian clock genes: effects on dopamine, reward and addiction. Alcohol. 2015; 49:341–349. [PubMed: 25641765]
50. Winton-Brown TT, Fusar-Poli P, Ungless MA, Howes OD. Dopaminergic basis of salience dysregulation in psychosis. Trends Neurosci. 2014; 37:85–94. [PubMed: 24388426]
51. Deacon RM. Assessing nest building in mice. Nat. Protoc. 2006; 1:1117–1119. [PubMed: 17406392]
52. Palchykova S, Winsky-Sommerer R, Meerlo P, Dürr R, Tobler I. Sleep deprivation impairs object recognition in mice. Neurobiol. Learn. Mem. 2006; 85:263–271. [PubMed: 16423541]
53. Anaclet C, et al. The GABAergic parafacial zone is a medullary slow wave sleep-promoting center. Nat. Neurosci. 2014; 17:1217–1224. [PubMed: 25129078]
54. Carter ME, et al. Tuning arousal with optogenetic modulation of locus coeruleus neurons. Nat. Neurosci. 2010; 13:1526–1533. [PubMed: 21037585]
55. Jego S, et al. Optogenetic identification of a rapid eye movement sleep modulatory circuit in the hypothalamus. Nat. Neurosci. 2013; 16:1637–1643. [PubMed: 24056699]

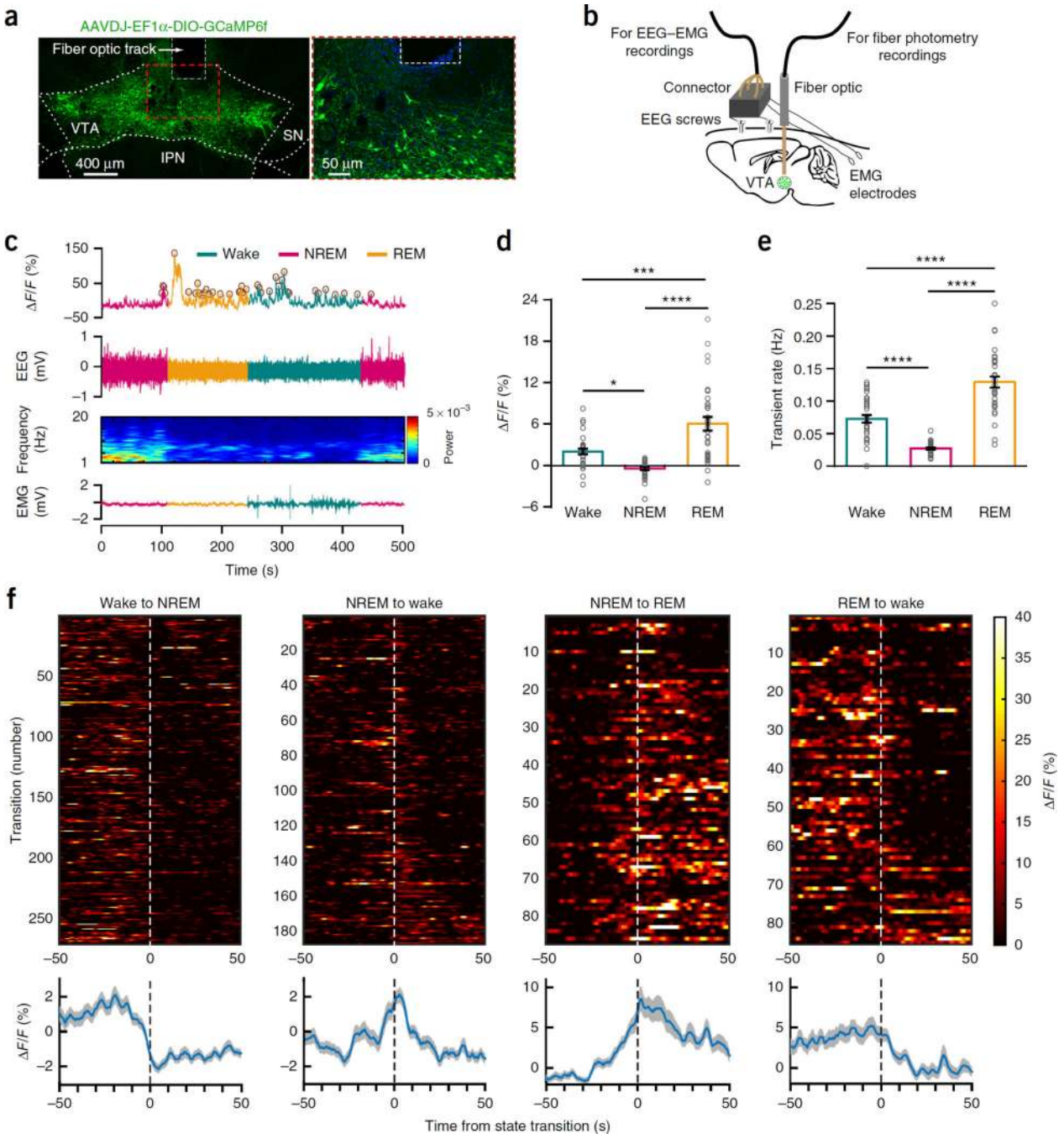

Figure 1.

Population activity of *Th*$^{+}$ VTA neurons across sleep–wake states, (**a**) Representative images of the VTA from a GCaMP6f-expressing mouse, showing viral expression and the placement of the tip of the fiber above the VTA (one of four mice), (**b**) Schematic of the *in vivo* recording configuration, (**c**) Representative fluorescence trace, EEG, EEG power spectrogram and EMG trace across spontaneous sleep–wake states. Δ*F/F*, change in fluorescence from median of the entire time series. Brown circles, transients detected using a filtering-based algorithm. (**d,e**) Mean ± s.e.m. fluorescence (**d**) and transient rate (**e**) during

wake, NREM sleep and REM sleep ($n = 4$ mice, 8 sessions per mouse; two-way repeated-measures (RM) ANOVA between arousal state and mice, arousal state: $F_{2,14} = 36.95$ (fluorescence) and 89.26 (transient rate), $P = 2.6 \times 10^{-6}$ (fluorescence) and 1.08×10^{-8} (transient rate); followed by Tukey's *post hoc* tests, *$P = 0.015$, ***$P = 3 \times 10^{-4}$, ****$P = 1 \times 10^{-6}$ (fluorescence) and ****P(wake-NREM) $= 9 \times 10^{-5}$, (wake–REM) $= 9 \times 10^{-6}$ and (NREM–REM) $= 6 \times 10^{-9}$. (**f**) Fluorescence aligned to arousal state transitions. Top, individual transitions with color-coded fluorescence intensity (wake-NREM, $n = 254$; NREM-wake, $n = 172$; NREM–REM, $n = 86$; REM-wake, $n = 84$). Bottom, average responses from all the transitions expressed as mean (blue trace) ± s.e.m. (gray shading). Trials in top panel are sorted by the duration of the second state (shortest, top; longest, bottom).

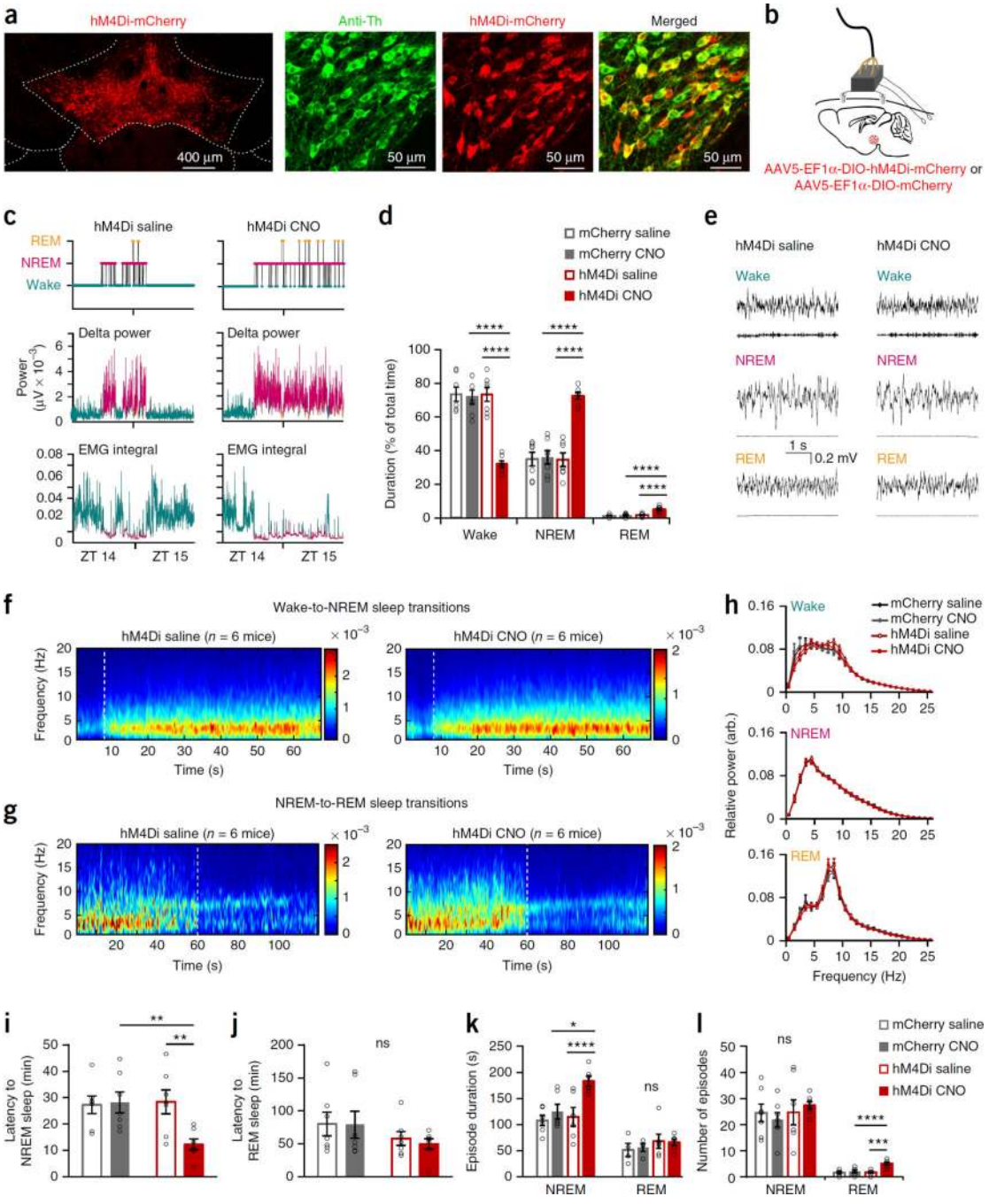

Figure 2.

Chemogenetic inhibition of *Th*$^{+}$ VTA neurons decreases wakefulness and increases sleep. (**a**) hM4Di expression in the VTA and co-expression of mCherry in *Th*$^{+}$ cells (one of seven mice). (**b**) Schematic of injection and implant. (**c**) Hypnogram, fast Fourier transform–derived delta power and EMG activity over 2 h after injection (one of seven mice). (**d**) Percent (mean ± s.e.m.) time in wake, NREM and REM sleep during 2 h after njection (n = 7 per group, two-way RM ANOVAs between compound injected and virus, interaction: $F_{1,12}$ = 41.96 (wake), 42.03 (NREM), 9.64 (REM); $P = 3 \times 10^{-5}$ (wake and NREM), 0.0091

(REM)). (**e**) Representative EEG-EMG traces. EEG power spectrogram (μV) of (**f**) wake-to-NREM sleep transitions and (**g**) NREM-to-REM sleep transitions (aligned to state transition at 8 s and 60 s, respectively; dashed white line). Presented are averages across all transitions (wake-to-NREM, $n = 99$ transitions (saline) and $n = 138$ (CNO); NREM-to-REM $n = 10$ (saline) and $n = 30$ (CNO)), in all mice ($n = 6$ per group). (**h–l**) Sleep–wake parameters (mean ± s.e.m.) during the 2 h after injection ($n = 7$ per group, two-way RM ANOVAs followed by Sidak's *post hoc* tests, *$P = 0.011$, **P(CNO: mCherry-hM4Di) = 0.009 and (hM4Di: saline-CNO) = 0.001, ***$P = 2 \times 10^{-4}$, ****P(NREM–hM4Di: saline–CNO) = 7×10^{-5}, ****P(REM-CNO: mCherry-hM4Di) = 5×10^{-5}. (**h**) EEG power spectrum of arousal states episodes (two-way RM ANOVAs between compound injected and frequency, compound injected: $P > 0.18$). (**i,j**) Latency to the first (**i**) NREM and (**j**) REM sleep episode (interaction: $F_{1,12} = 11.03$ (NREM), 0.16 (REM); $P = 0.006$ (NREM), 0.96 (REM)). (**k**) Duration of individual arousal state episodes (interaction: $F_{1,12} = 13.83$ (NREM), 0.15 (REM); $P = 0.004$ (NREM), 0.71 (REM)). (**l**) The total number of arousal state episodes (interaction: $F_{1,12} = 0.93$ (NREM), 15.52 (REM); $P = 0.35$ (NREM), 0.002 (REM)).

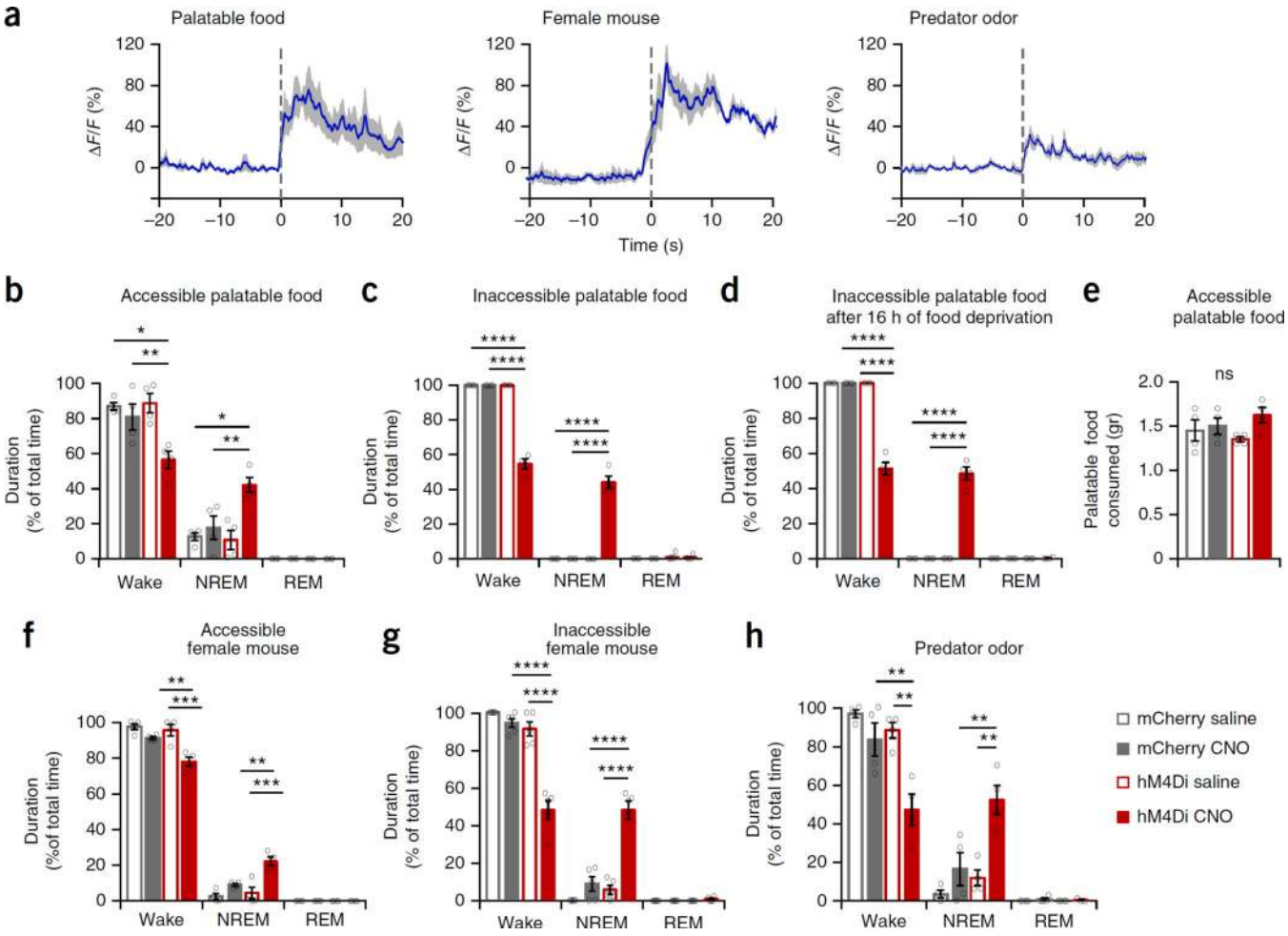

Figure 3.

Activity in *Th*$^{+}$ VTA neurons is necessary for wake maintenance even in the face of salient stimuli, (**a**) *Th*$^{+}$ VTA neurons population activity in response to salient stimuli. Time 0 represents contact with food or predator odor and the placement of the female mouse in the cage. Presented are average responses ($n = 4$ mice; blue trace) ± s.e.m. (gray shading). (**b-d,f-h**) Percent time in wake, NREM and REM sleep (mean ± s.e.m.; $n = 4$ per group for **b-d,f,h** and $n = 5$ for **g;** two-way RM ANOVA between compound injected and viral transduction, followed by Sidak's *post hoc* test; *$P < 0.05$, **$P < 0.01$, ***$P < 0.001$, ****$P < 0.0001$. (**b**) In the presence of high-fat chow (interaction: $F_{1,6} = 6.75$ (wake) and 7.58 (NREM), $P = 0.04$ (wake) and 0.03 (NREM)). (**c,d**) In the presence of inaccessible high-fat chow (**c**) in normally fed mice (interaction: $F_{1,6} = 241.3$ (wake) and 162.1 (NREM), $P = 4.5 \times 10^{-6}$ (wake) and 1.4×10^{-5} (NREM)) and (**d**) in 16-h food-deprived mice (interaction: $F_{1,6} = 193.1$ (wake) and 173.1 (NREM), $P = 8.65 \times 10^{-6}$ (wake) and 1.9×10^{-5} (NREM)). (**e**) Amount (mean ± s.e.m.) of high-fat chow consumed during a 1-h test period in the presence of 6 g high-fat chow (interaction: $F_{1,6} = 1.45$, $P = 0.27$). (**f**) In the presence of a freely moving female mouse (interaction: $F_{1,6} = 12.31$ (wake) and 12.56 (NREM), $P = 0.01$ for wake and NREM)). (**g**) In the presence of an inaccessible female mouse (interaction: $F_{1,8} = 50.22$ (wake) and 34.97 (NREM), $P = 0.0001$ (wake) and 3.5×10^{-4} (NREM)). (**h**) In the

presence of a predator odor (virus: $F_{1,6}$ = 13.9 (wake) and 14.75 (NREM), P= 0.0098 (wake) and 0.0086 (NREM); compound injected: $F_{1,6}$ = 16.9 (wake) and 17.47 (NREM), P= 0.0063 (wake) and 0.0058 (NREM)).

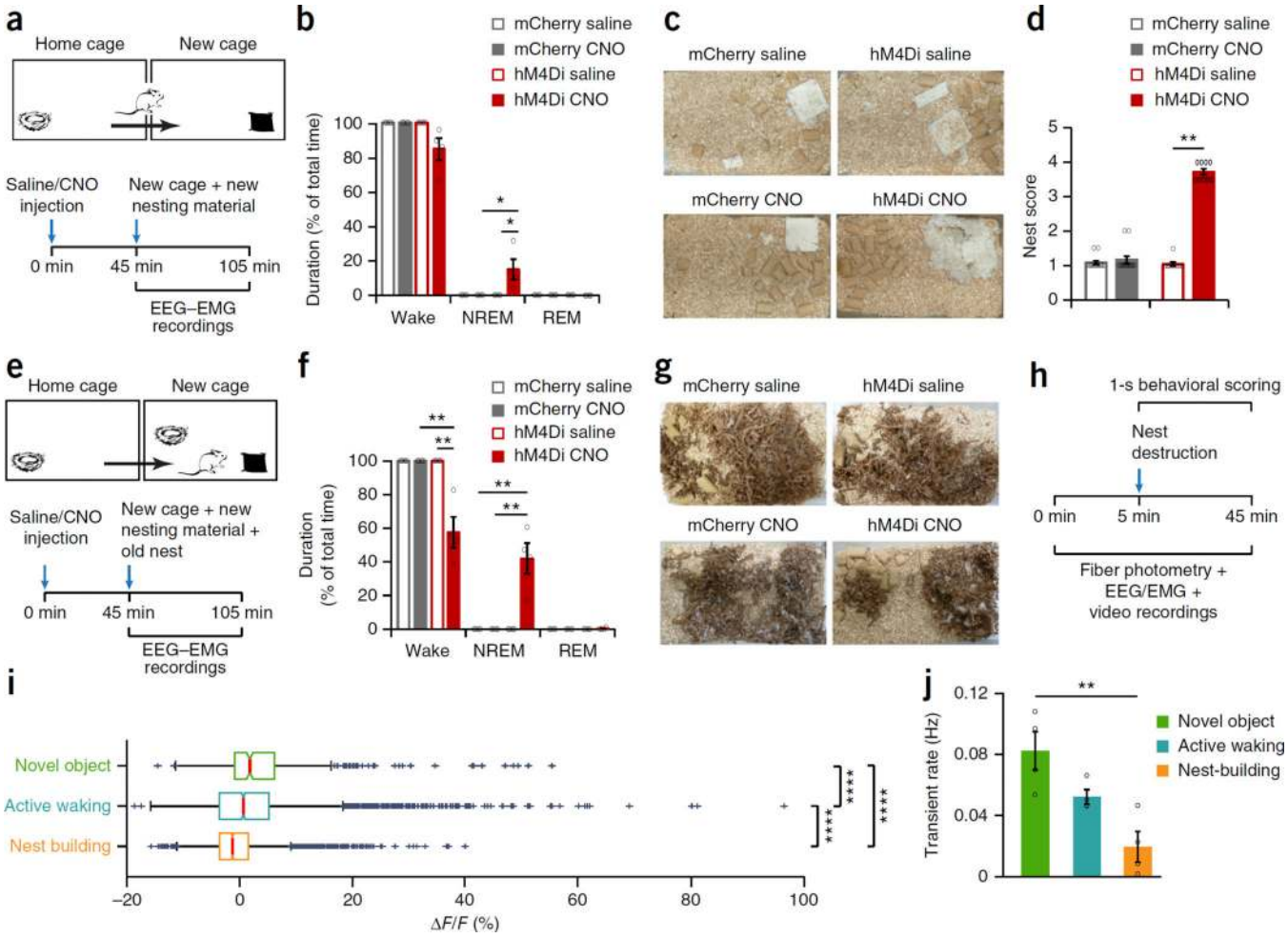

Figure 4.

Chemogenetic inhibition of *Th*$^{+}$ VTA neurons promotes nest-building behavior. (**a**) Diagram of experiment. (**b**) Percentage (mean ± s.e.m.) of time spent awake, in NREM sleep and in REM sleep following the transfer to a new cage in mCherry and hM4Di mice ($n = 4$ per group). Two-way RM ANOVA between compound injected and viral transduction, interaction: $F_{1,6} = 5.847$ (wake) and 6.328 (NREM), $P = 0.052$ (wake) and 0.0456 (NREM); followed by Sidak's *post hoc* tests, **P*(hM4Di: saline–CNO) = 0.02, (CNO: mCherry-hM4Di) = 0.007. (**c**) Representative pictures of mCherry and hM4Di mouse cages following saline (top) and CNO (bottom) injections at the end of the 1-h test period (one each of 13 mCherry and 9 hM4Di mice). (**d**) Nesting score (mean ± s.e.m.) represents the amount of nesting material used and shape of the nest during the 1-h test period (1, poor; 5, good). Wilcoxon matched-pairs signed rank test, mCherry: $n = 13$, $W = 3$, $P = 0.75$; hM4Di: $n = 9$, $W = 45$, **$P = 0.0039$. (**e**) Diagram of experiment. (**f**) Percentage (mean ± s.e.m.) of time spent awake, in NREM and REM sleep during the test hour following the transfer to a new cage, in mCherry and hM4Di mice ($n = 4$ per group). Two-way RM ANOVA between compound injected and viral transduction, followed by Sidak's *post hoc* tests: *P*(CNO: mCherry–hM4Di) = 5×10^{-5} and (hM4Di: saline–CNO) = 0.001. (**g**) Representative pictures of mCherry and hM4Di mouse cages following saline (top) and CNO (bottom)

injections, at the end of the 1-h test period ($n = 4$ mice each). (**h**) Timeline of experiment. (**i**) Fluorescence changes during novel object exploration, active waking and nest-building, calculated per 1-s epoch. Box plot: central mark indicates median; bottom and top edges indicate the 25th and 75th percentiles, respectively. The whiskers extend to the most extreme data points not considered outliers, and the outliers are plotted ndividually using the "+" symbol. From 4 mice, novel object, $n = 374$ epochs; active waking $n = 2{,}801$ epochs; nest-building $n = 2{,}143$ epochs), two-way ANOVA between behavioral state and mice, behavioral state: $F_{3,2} = 37.25$, $P = 5.2 \times 10^{-50}$; followed by Sidak's *post hoc* tests, P(active waking-novel object) = 1×10^{-5}, (active waking–nest building) = 9×10^{-10} and (novel object–nest building) = 9×10^{-10}. (**j**) Mean (± s.e.m.) transient rate during novel object exploration, active waking and nest-building ($n = 4$ mice). One-way ANOVA; $F_{2,9} = 10.56$, $P = 0.0044$; followed by Tukey's multiple comparisons test, $^{**}P = 0.0033$

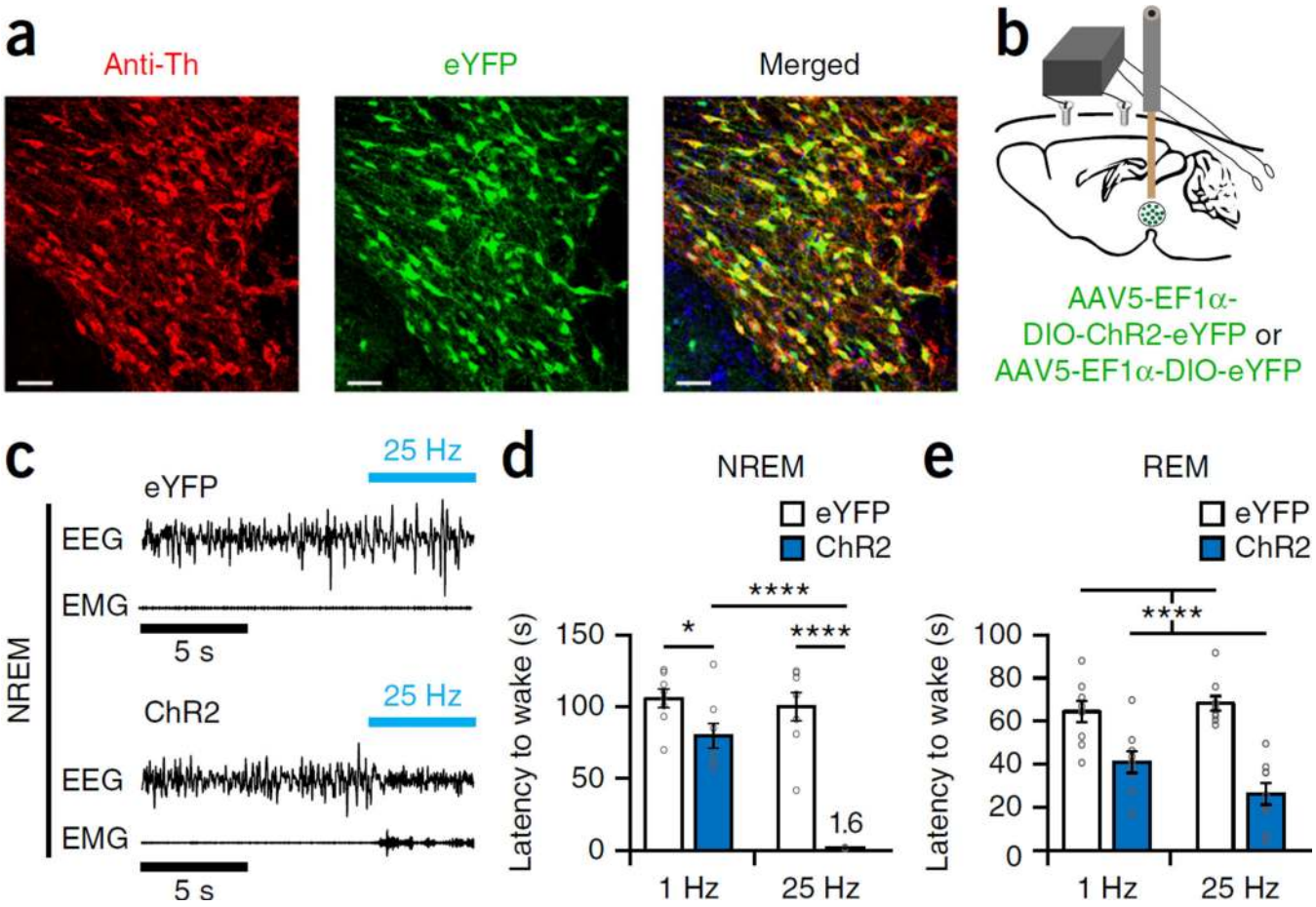

Figure 5.

Optogenetic activation of *Th*$^{+}$ VTA neurons is sufficient to initiate wakefulness. (**a**) Representative immunofluorescence image of the VTA from an eYFP mouse, showing expression of the fluorescent protein eYFP and *Th*$^{+}$ cells of the VTA. Scale bar, 50 μm (one of eight mice). (**b**) Schematic of injection and implant. (**c**) Representative traces of EEG-EMG recordings showing an immediate sleep-to-wake transition during NREM sleep after acute photostimulation (25 Hz for 5 s) of *Th*$^{+}$ VTA neurons during the inactive (light) phase in a mouse transduced with ChR2 (bottom) but not in a mouse transduced with eYFP (top). (**d**) Mean latency (± s.e.m.) to wake from NREM sleep following optogenetic stimulation at 1 and 25 Hz of eYFP (white) and ChR2 (blue) mice ($n = 8$ per group; 6–10 stimulations per frequency per mouse). Two-way RM ANOVA between stimulation condition and viral transduction; $F_{1,14} = 63.27$ (virus), 38 (frequency) and 28.34 (interaction), $P = 1.4 \times 10^{-6}$ (virus), 2.5×10^{-5} (frequency) and 1×10^{-4} (interaction); followed by Sidak's *post hoc* tests, *$P = 0.035$, ****P(ChR2: 1 HzαΔ±μ–25 Hz) = 2×10^{-6} and P(25 Hz: eYFP–ChR2) = 5×10^{-10}. (e) Mean latency (± s.e.m.) to wake from REM sleep following optogenetic stimulation at 1 and 25 Hz of eYFP (white) and ChR2 (blue) mice ($n = 9$ per group; 6–10 stimulations per frequency per mouse). Two-way RM ANOVA between stimulation condition and viral transduction; $F_{1,16} = 59.25$ (virus), 1.2 (frequency) and 3.45 (interaction), $P = 1 \times 10^{-6}$ (virus), 0.29 (frequency) and 0.08 (interaction).

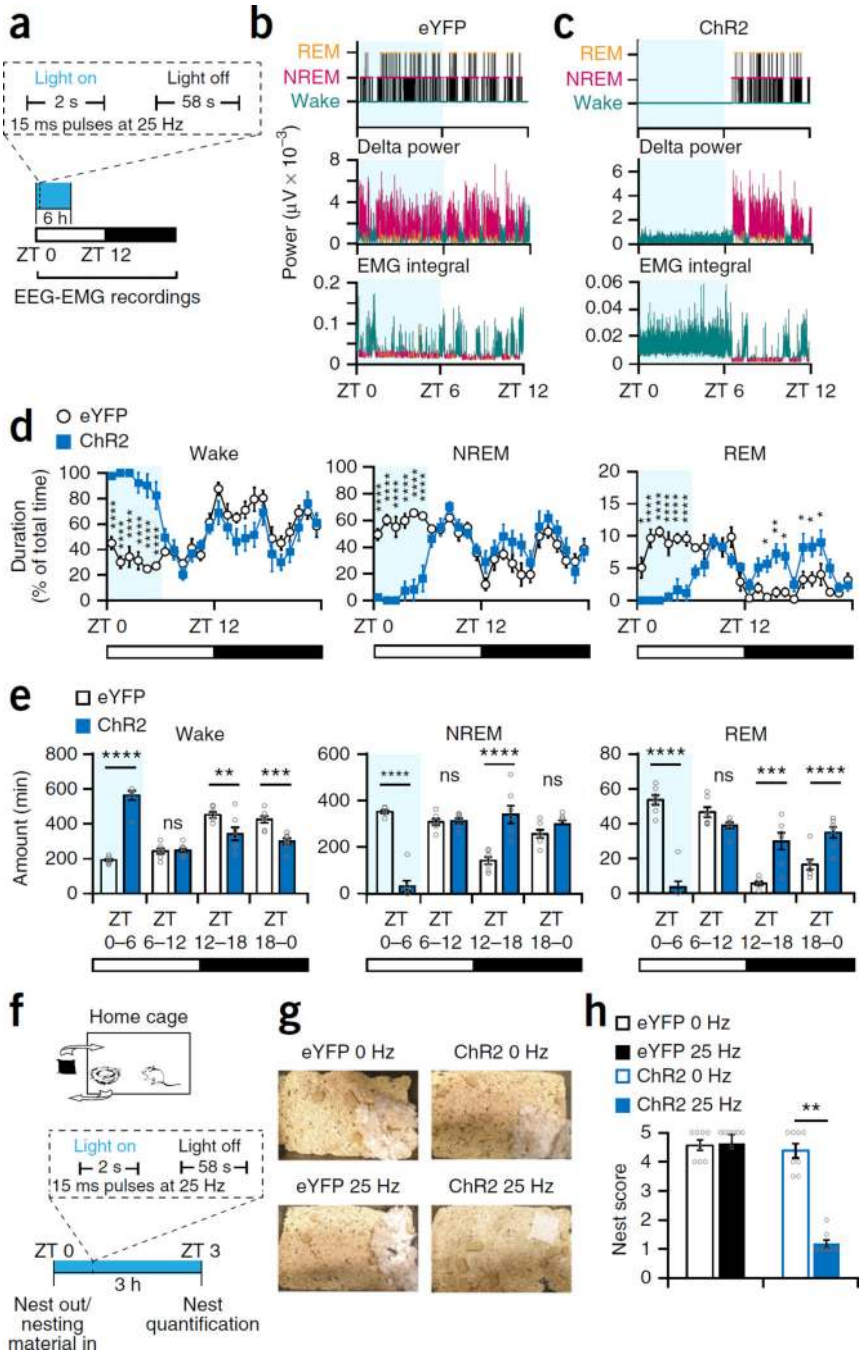

Figure 6.

Optogenetic activation of *Th*+ VTA neurons is sufficient to maintain wakefulness and suppress nest-building behavior. (**a**) Diagram of stimulation protocol. (**b,c**) Representative hypnogram, fast Fourier transform–derived delta power and EMG activity over the 12 h of the nactive, light phase in (**b**) an eYFP and (**c**) a ChR2 mouse. Light blue shading represents the stimulation phase. (**d**) Percent (mean ± s.e.m.) time spent awake (left), in NREM sleep (middle) and REM sleep (right) during 24 h, starting with the photostimulation ($n = 7$ per group; two-way RM ANOVA between time and viral transduction, interaction: $F_{23,138}$ =

11.65 (wake), 10.38 (NREM), and 12.18 (REM), $P = 1 \times 10^{-15}$ for wake, NREM and REM sleep; followed by Sidak's *post hoc tests*, Wake: P(ZT 0) = 3×10^{-6}, P(ZT 1) = 3×10^{-10}, P(ZT 2) = 4×10^{-9}, P(ZT 3) = 5×10^{-8}, P(ZT 4) = 5×10^{-9}, P(ZT 5) = 1×10^{-6}; NREM: P(ZT 0) = 3×10^{-6}, P(ZT 1) = 1×10^{-9}, P(ZT 2) = 3×10^{-8}, P(ZT 3) = 1×10^{-7}, P(ZT 4) = 9 × 10-9, P(ZT 5) = 4×10^{-6}; REM: P(ZT 0) = 0.02, P(ZT 1) = 1×10^{-7}, P(ZT 2) = 3×10^{-9}, P(ZT 3) = 8×10^{-6}, P(ZT 4) = 2×10^{-5}, P(ZT 5) = 5×10^{-6}, P(ZT 14) = 0.025, P(ZT 15) = 0.003, P(ZT 16) = 0.01, P(ZT 18) = 0.03, P(ZT 19) = 0.03, P(ZT 20) = 0.03. (**e**) Duration (mean ± s.e.m.) per 6-h bin; $n = 7$ per group; two-way RM ANOVA between time and viral transduction; interaction: $F_{3,36} = 54.92$ (wake), 81.64 (NREM), and 56.8 (REM), P = 1.6×10^{-13} (wake), 1×10^{-15} (NREM), and 9.9×10^{-14} (REM). (f) Diagram of experiment. (g) Representative pictures of the cages of eYFP and ChR2 mice at the end of the 3-h stimulation period at 0 Hz and 25 Hz (one of eight each). (**h**) Nesting score (mean ± s.e.m.); $n = 8$ mice per group, Wilcoxon matched-pairs signed rank test; eYFP: $W = 0$, $P = 0.99$; ChR2: $W = -36$, $^{**}P = 0.0078$.

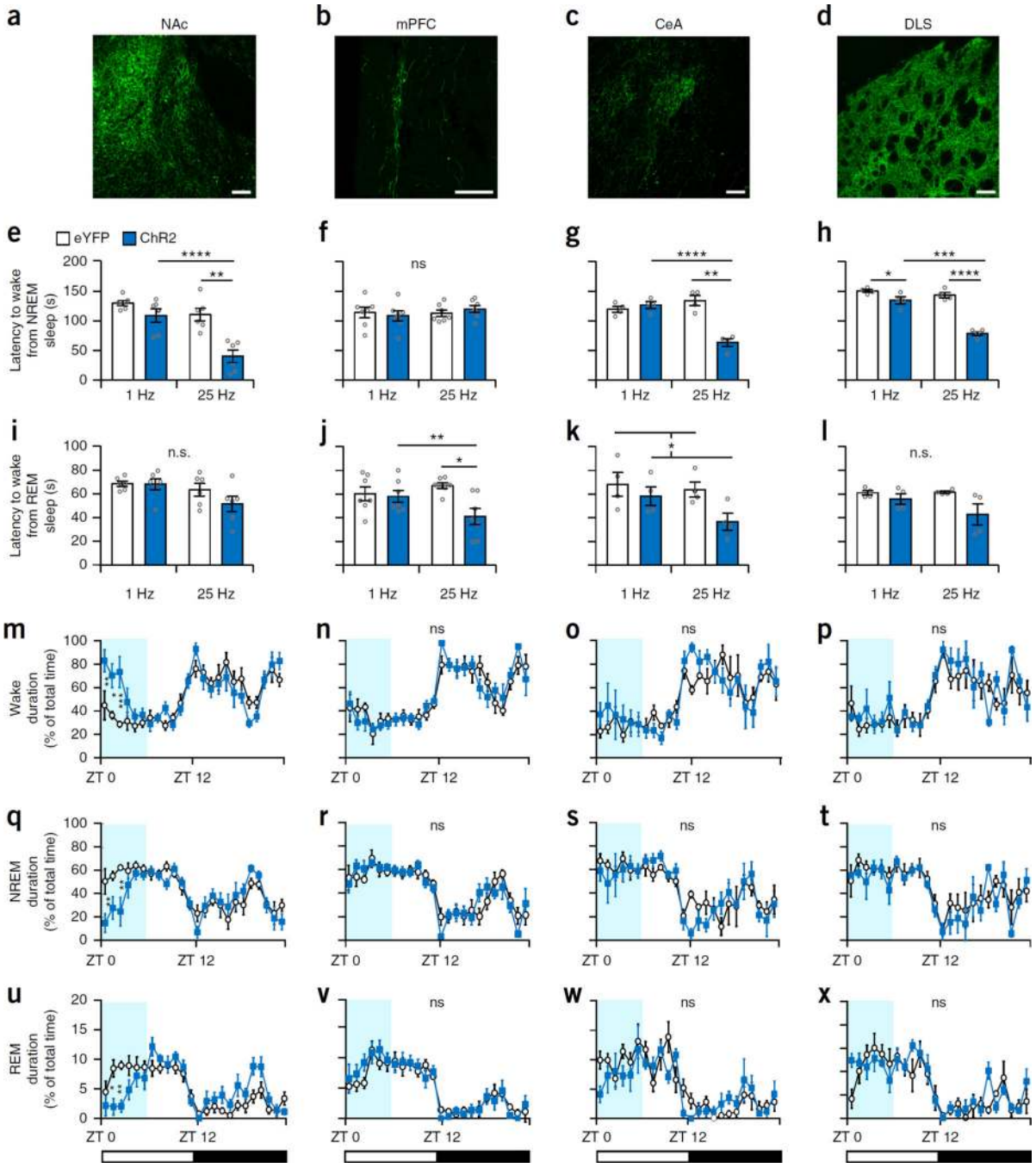

Figure 7.

Th^{+} VTA neuron projections differentially modulate arousal. (**a–d**) Representative images of *Th*$^{+}$ VTA fibers expressing ChR2 at the (**a**) NAc, (**b**) mPFC, (**c**) CeA and (**d**) DLS. Scale bars, 100 μm (one of six mice for **a** and **b** and one of four mice for c and **d**). Note that each column represents one output region. (**e–h**) Mean latency (± s.e.m.) to wake from NREM sleep following optogenetic stimulation at 1 and 25 Hz of eYFP and ChR2 mice (8–12 stimulations per frequency per mouse); two-way RM ANOVA between frequency and viral transduction (interactions: $F_{1,10} = 5.4$ (NAc), $F_{1,12} = 0.94$ (mPFC), $F_{1,6} = 31.71$ (CeA), $F_{1,6}$

= 29.73 (DLS), P(NAc) = 0.042, P(mPFC) = 0.35, P(CeA) = 0.001, P(DLS) = 0.002), followed by Sidak's *post hoc* tests (NAc: $^{**}P = 0.002$, $^{****}P = 9 \times 10–^{6}$, CeA: $^{**}P = 0.001$, $^{****}P = 1 \times 10^{-5}$, DLS: $^{*}P = 0.046$, $^{***}P = 2 \times 10^{-4}$, $^{****}P = 4 \times 10^{-7}$). (i–l) Mean atency (± s.e.m.) to wake from REM sleep following optogenetic stimulation at 1 and 25 Hz of eYFP and ChR2 mice (8–12 stimulations per frequency per mouse); two-way RM ANOVA between frequency and viral transduction (interactions: $F_{1,10} = 0.8$ (NAc), $F_{1,12} = 5.081$ (mPFC), $F_{1,6} = 1.032$ (CeA), $F_{1,6} = 1.94$ (DLS); P(NAc) = 0.3, P(mPFC) = 0.043, P(CeA) = 0.35 , P(DLS) = 0.2; virus (CeA): $F_{1,6} = 6.207$, $P = 0.047$) followed by Sidak's *post hoc* tests (mPFC: $^{**}P = 0.003$, $^{****}P = 9 \times 10^{-6}$). (**m**–**x**) The percentage (mean ± s.e.m.) of time spent (**m**–**p**) awake, (**q**–**t**) in NREM sleep and (**u**–**x**) in REM sleep during 24 h starting with photostimulation of the different output regions in eYFP (white) and ChR2 (blue) mice. n = 6 per group for NAc and mPFC and $n = 4$ per group for CeA and DLS experiments; two-way RM ANOVA between time and viral transduction (NAc interactions: wake $F_{23,115} = 2.829$, $P = 0.0001$; NREM $F_{23,115} = 2.455$, $P = 0.0009$; REM: $F_{23,115} = 2.938$, $P = 8 \times 10^{-5}$), followed by Sidak's *post hoc tests* (NAc wake: P(ZT 0) = 0.005, P(ZT 1) = 0.022, P(ZT 2) = 0.0004; NREM: P(ZT 0) = 0.003, P(ZT 2) = 0.001; REM: P(ZT 1) = 0.01, P(ZT 2) = 0.005).